Propagation failure dynamics of wave trains in excitable systems

Niklas Manz,* Brent T. Ginn, and Oliver Steinbock†
Department of Chemistry and Biochemistry, Florida State University, Tallahassee, Florida 32306-4390, USA
(Received 30 January 2006; published 22 June 2006)

We report experimental and numerical results on temporal patterns of propagation failures in reaction-diffusion systems. Experiments employ the 1,4-cyclohexanedione Belousov-Zhabotinsky reaction. The propagation failures occur in the frontier region of the wave train and can profoundly affect its expansion speed. The specific rhythms observed vary from simple periodic to highly complex and possibly chaotic sequences. All but the period-1 sequences are found in the transition region between "merging" and "tracking" dynamics, which correspond to wave behavior caused by two qualitatively different types of anomalous dispersion relations.

DOI: 10.1103/PhysRevE.73.066218 PACS number(s): 82.40.Ck, 82.20.Wt, 05.45.−a

I. INTRODUCTION

Propagating fronts and wave trains exist in a broad variety of nonlinear systems that span the entire range of science and engineering disciplines [1]. Examples include crystallization fronts [2,3], action potentials on neurons [4], spreading epidemics [5], and traveling stripes on the skin of a mutant mouse [6]. In excitable reaction-diffusion (RD) media [7], propagating fronts are also the building blocks of more complex spatio-temporal patterns such as rotating vortices [8,9] and three-dimensional scroll waves [10,11] with the latter being related to cardiac arrhythmias [12,13]. All of these wave phenomena are governed, or at least strongly influenced, by the specific interactions between the individual wave pulses and the investigation of pulse interaction is therefore of central importance.

Pulse interaction is typically discussed in terms of dispersion relations. The classic approach is to analyze the stability and the velocity c of infinite wave trains as a function of their wavelength λ. Most excitable RD systems have monotonically increasing dispersion relations $c(\lambda)$ that converge to the velocity of solitary pulses for large wavelengths. Furthermore, the refractory zone of excitation pulses gives rise to a minimal wavelength below which no wave propagation occurs. Such normal dispersion relations have been identified for numerous experimental systems including the widely studied Belousov-Zhabotinsky (BZ) reaction [14–16].

Already in the 1980s, theoretical and numerical investigations of excitable RD models revealed anomalous dispersion relations that involve a single overshoot of $c(\lambda)$ or damped oscillations [17,18]. These anomalies are especially likely in systems that have a stable focus as their excitable rest state. The first convincing experimental examples for nonmonotonic dispersion in excitable systems were measured using chemical reactions, namely the oxidation of CO [19] and the catalytic reduction of NO with CO [20] on Pt(100) surfaces as well as the homogeneously catalyzed 1,4-cyclohexanedione-Belousov-Zhabotinsky (CHD-BZ) reaction [21–23]. However, we note that this phenomenon also exists in biological systems, such as neuronal tissue [24], for which it is commonly referred to as "super-normal excitability."

The analysis of infinite wave trains does not always unravel the rich dynamics of finite wave trains. An important example is the motion of step defects during the growth, the sublimation and the dissolution of certain crystals such as silicon [25,26], potassium dihydrogen phosphate (KDP) [27,28], and gallium arsenide [29,30]. Under certain conditions, the defects obey anomalous dispersion relations that cause attractive interaction between neighboring steps. The resulting aggregation process is known as "step bunching" and can lead to the formation of macroscopic defects that severely compromise the quality of semiconductors, laser materials, and protein crystals. A similar phenomenon, coined "wave stacking," is observed in the CHD-BZ reaction [21,22]. Figure 1(a) shows a typical time-space plot that illustrates the formation of densely stacked pulse packets in the wake of a slow leading pulse. All pulses nucleate at an oscillatory pacemaker around $x=0$. Analogous behavior exists in pseudo-two-dimensional CHD-BZ media as exemplified by the snapshot in Fig. 1(b).

Step bunching and wave stacking are governed by anomalous dispersion relations and yield structures with a characteristic wavelength λ_0. This distance must obey the stability criterion $dc(\lambda_0)/d\lambda > 0$ and $c(\lambda_0)=c_0$ where c_0 is the speed of the solitary pulse or step. However, the minimal wavelength of the dispersion curve can be larger than λ_0. Under these conditions, trailing pulses approach the leading pulse and vanish in a front-to-back collision. This behavior is referred to as "wave merging" and has been observed in a catalytic surface reaction [19,20] and in the CHD-BZ system [21,22]. Typical examples obtained from one- and two-dimensional CHD-BZ systems are shown in Figs. 1(c) and 1(d), respectively.

Recent numerical studies have revealed other dispersion anomalies. These include bistability in a model of the BZ reaction [31] and band gaps in a model of intracellular Ca^{2+} dynamics [32]. Furthermore, our group reported the existence of finite bandwidth dispersion curves in the CHD-BZ reaction [33,34]. In such systems, the wavelength of pulse trains must fall between a minimal and a maximal wavelength, while all other structures, including solitary pulses,

*Present address: Neurodynamics Laboratory, Department of Psychiatry, SUNY, Downstate Medical Center, 450 Clarkson Avenue, Brooklyn, NY 11203.
†Electronic address: steinbck@chem.fsu.edu

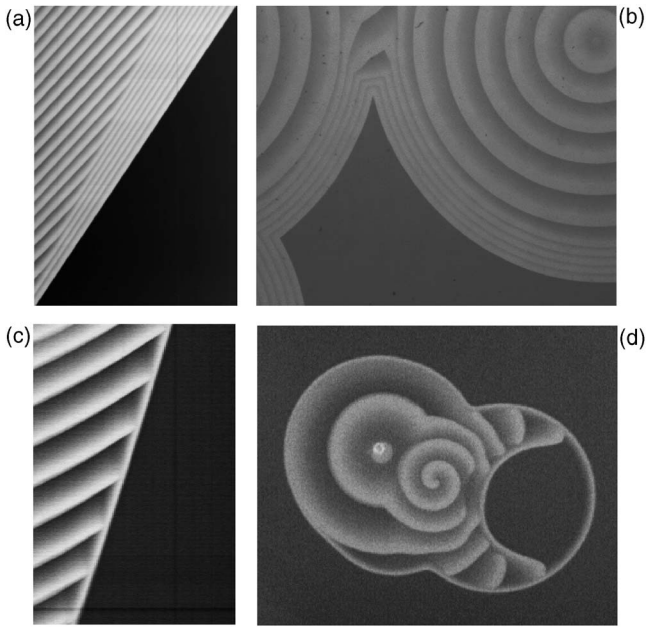

FIG. 1. Examples of stacking (a, b) and merging (c, d) dynamics. Space-time plots of wave propagation in quasi-one-dimensional systems (a, c) and snapshots of waves in two-dimensional systems (b, c). Initial concentrations: $[H_2SO_4]=2.00M$ (a, b) and $0.60M$ (c, d), $[CHD]=0.11M$, $[NaBrO_3]=0.07M$ (a, b) and $0.10M$ (c, d), and [ferroin]=0.5 mM. The horizontal and vertical axes span 11.7 mm and 224 s (a) and 9.5 mm and 500 s (c), respectively. Field of view: (20.1×16.7) mm^2 (b) and (25.0×20.3) mm^2 (d).

are unstable. Moreover, finite wave trains undergo repeated annihilation events of their leading pulses. Nonetheless, such wave trains grow in size as each annihilated pulse has "cleared the way," so that subsequent fronts can propagate farther. We therefore refer to this type of front dynamics as "wave tracking." Exemplary space-time plots of this behavior are shown in Figs. 2(a) and 2(b) for a one-dimensional system and in Fig. 2(d) for a two-dimensional system.

This paper presents quantitative measurements concerning wave merging and wave tracking. In particular, we describe unusual propagation failures and firing sequences that are characteristic for conditions between merging and tracking. Experimental observations are modeled and complemented by numerical simulations using simple, three-variable reaction-diffusion equations.

II. EXPERIMENTAL

A modified BZ reaction with 1,4-cyclohexanedione as the organic substrate [35,36] and either ferroin or $Fe[batho(SO_3)_2]_3$ as the redox catalyst and indicator is used to perform the experiments. Aqueous stock solutions of $2.0M$ sodium bromate (Fluka) and $0.5M$ 1,4-cyclohexanedione (Aldrich) are prepared in nanopure water (18 MΩ cm) obtained from a Barnstead EASYpure UV unit. The CHD solution is filtered through a Whatman 0.2 μm NYL filter. Sulfuric acid (5.0M, Riedel-de Haën) and ferroin (25 mM, Fluka) are purchased as standardized solution and used without further purification. $Fe[batho(SO_3)_2]_3$ is prepared in a

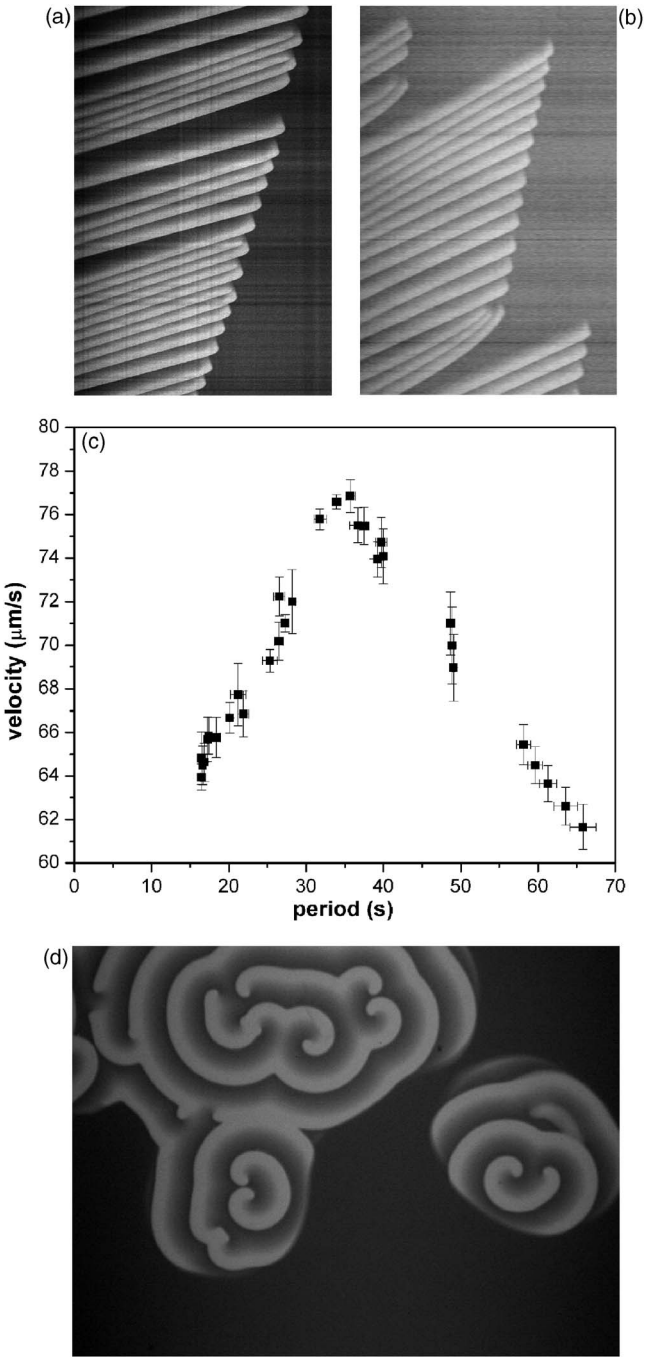

FIG. 2. Wave dynamics in the tracking regime. Space-time plots of wave propagation in quasi-one-dimensional systems (a,b), a dispersion relation (c) evaluated from (a), and a snap-shot of waves in a two-dimensional system (d). Initial concentrations: $[H_2SO_4]=0.6M$, $[CHD]=0.20M$ (a, b) and $0.11M$ (d), $[NaBrO_3]=0.20M$ (a, b), and $0.10M$ (d), and $[Fe[batho(SO_3)_2]_3]=0.5$ mM. The horizontal and vertical axes span 8.1 mm and 600 s (a) and 13.1 mm and 570 s (b). Field of view in (d): (21.2×13.0) mm^2.

25 mM sulfuric acid solution by mixing a 3:1 molar ratio of 4,7-diphenyl-1,10-phenanthrolinedisulfonic acid disodium salt hydrate (Acros) with ferrous sulfate heptahydrate (Fluka) to yield the complex at a concentration of 25 mM.

Quasi-one-dimensional experiments are carried out in capillaries (Drummond 20 μL MICROCAPS®) with a length

of 64 mm and an inner diameter of 0.63 mm for which the dynamics within the system can be considered pseudo-one-dimensional. Snap-shots of waves in quasi-two-dimensional systems are obtained using batch reactors in which the solution is confined between two planar polystyrene plates spaced at 0.4 mm. Absorption profiles are monitored with a monochrome charge-coupled-device camera (COHU 2122; 640×480 pixel, 8 bit per pixel). The video signal is digitized with a low-noise image-acquisition card (Data Translation DT3155). Image data are acquired every (0.25–1.00) s as bitmap images using commercial software (HLImage++97). For image analysis we use programs written in IDL (Interactive Data Language, Research System Inc., Version 5.2). All experiments are performed at (24 ± 1) °C.

III. EXPERIMENTAL RESULTS

Figure 2(a) illustrates the dynamics of tracking waves in a pseudo-one-dimensional CHD-BZ system. The vertical and horizontal axes represent time and space, respectively, with time evolving in upward direction. Within the time-space plot, each oxidation pulse generates one bright band. In this particular example, all wave pulses nucleate from an oscillatory defect at the left boundary of the system, the open end of the capillary, where bromine escapes from the solution into the ambient atmosphere. They show the main characteristics of tracking waves namely propagation failure after a finite distance that increases with each pulse annihilation, thus, causing an overall expansion of the wave pattern.

The expansion process can be described by the motion of a virtual boundary which connects the coordinates $x_n(t)$ at which the nth pulse vanishes. For the example shown in Fig. 2(a), the average velocity of this boundary is 6.3 μm/s and thus one order of magnitude slower than the average pulse speed of 70 μm/s. Furthermore, the expansion speed decreases with increasing times elapsed between an annihilation event and the arrival of the next pulse. This dependence is more pronounced for the experiment shown in Fig. 2(b). This time-space plot reveals a sawtooth-shaped expansion line of the wave train boundary and the wave train undergoes two major size reductions during the analyzed time interval. In between those "catastrophes," however, the pattern grows at a nearly steady rate.

Using the data in Fig. 2(a), we analyze the dependence of pulse speed c on the time elapsed between subsequent fronts, which we will refer to as the period T. To a certain extent these data are a good approximation of the system's dispersion relation. Figure 2(c) shows that pulse speeds vary in a nonmonotonic fashion between approximately 60 μm/s and 80 μm/s. Maximal speeds are found for periods around 35 s. Moreover, no wave pairs exist if the trailing front arrives at a given point less than 17 s after the leading front. This value is a good approximation of the lower end of the dispersion curve and corresponds to a minimal wavelength of about 1.1 mm.

In contrast to anomalous dispersion curves of stacking and merging waves, Fig. 2(c) reveals a maximal period above which no wave propagation occurs. For the given experimental conditions, we find this value to be 66 s. Consequently, the dispersion relation for tracking waves is limited to a finite band between 17 s and 66 s. To our knowledge, this is the first quantitative measurement of a finite bandwidth dispersion curve in a nonlinear RD system. There are numerous intriguing phenomena that result from this peculiar feature including the absence of stable solitary pulses. These phenomena also affect the wave dynamics in two-dimensional systems as exemplified by the snapshot shown in Fig. 2(d). Here, several spiral waves are organizing small domains filled with wave patterns. In contrast to common excitable systems, these domains are not bound by a continuous, closed front, but pulses annihilate and form numerous, nonrotating defects. The domains expand similarly to the one-dimensional wave trains shown in Figs. 2(a) and 2(b). However, preliminary analyses indicate that the local curvature of the domain boundary influences its growth velocity. This effect causes concave (convex) segments to expand slightly faster (slower) than planar boundary regions. In particular, concave segments are frequently encountered as they are formed in the collision-induced fusion of domains.

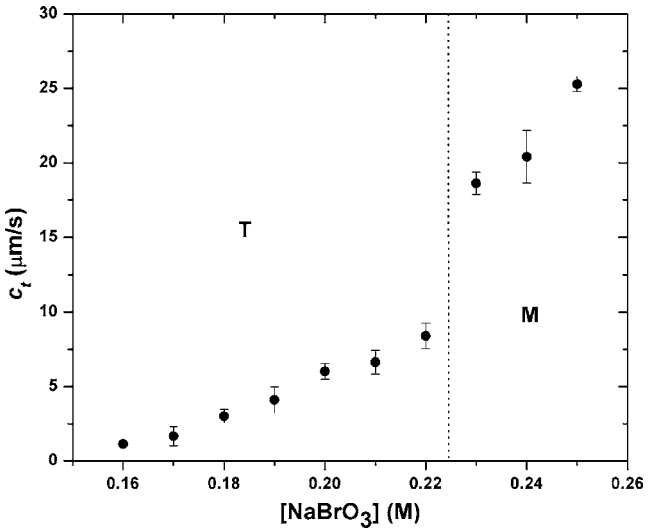

FIG. 3. Dependence of the tracking velocity c_t on $[NaBrO_3]$. At higher concentrations of $NaBrO_3$, i.e., in the merging regime, c_t becomes the velocity of the leading front. Other initial concentrations are the same as in Figs. 2(a) and 2(b).

An important feature of tracking waves is their ability to expand into wave-free regions through repeated pulse annihilation rather than through a stable, frontier pulse. This difference is also reflected in the typical expansion velocities of tracking waves. Figure 3 compares the average growth velocities of one-dimensional wave patterns for CHD-BZ systems with initial bromate concentration between 0.16M and 0.25M and otherwise identical conditions. This concentration range spans through the entire tracking and merging regime (labeled "T" and "M" in the figure, respectively). Below 0.16M no wave structures are observed, while concentrations above 0.25M yield stacking waves [cf. Figs. 1(a) and 1(b)]. Figure 3 shows that the expansion velocity of wave patterns increases with increasing concentration of bromate. Around 0.225M (dotted line), we observe the transition from tracking to merging waves. The transition is accompanied by a pro-

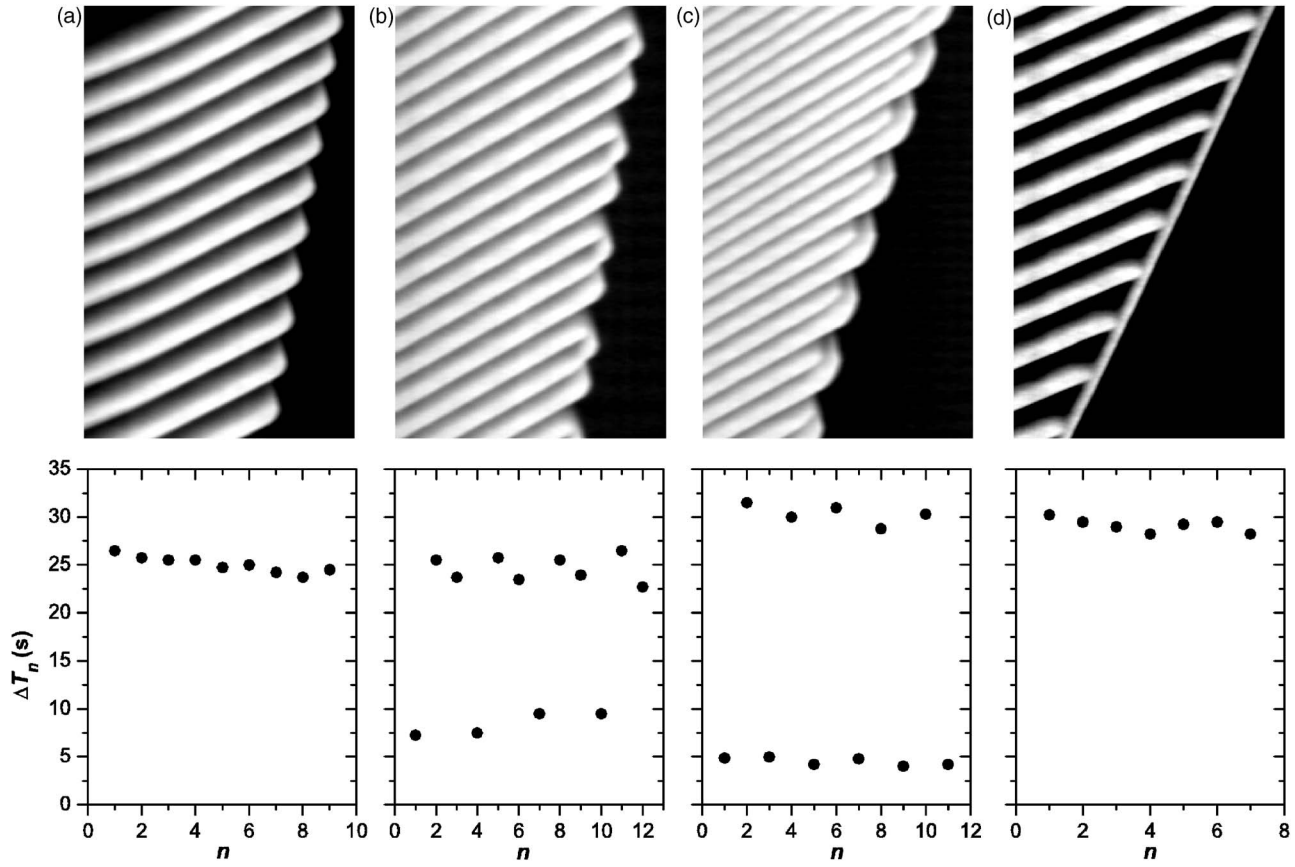

FIG. 4. Experimental space-time plots of wave dynamics in the transition region between tracking and merging and corresponding diagrams showing the time ΔT_n elapsed between the $(n-1)$st and the nth pulse death. Initial concentrations as in Figs. 2(a) and 2(b), except $[NaBrO_3]=0.21M$ (a), $0.22M$ (b), $0.23M$ (c), and $0.24M$ (d). The horizontal and vertical axes span 6.0 mm and 250 s, respectively.

found increase in the expansion velocity that nearly doubles from tracking (system's effective growth velocity) to merging (velocity of the slow propagating leading pulse). This result reemphasizes the qualitative differences between tracking and merging wave trains.

The growth of tracking wave patterns is closely tied to the pulses' ability of propagating slightly farther than their predecessors. This rather short but essential process suggests that the wave-free region is in a strongly inhibited state, while the concentration levels of this inhibitory species are greatly reduced within wave trains of sufficiently short wavelength. The overall tracking wave pattern grows at a constant speed c_t which depends on the wavelength of the wave train λ_i, the decay length Λ_i of pulses entering the steady-state medium at the leading edge of the pattern as well as on their average speed c_i within the pulse train [33,34] as follows:

$$c_t = c_i \frac{\Lambda_i}{\Lambda_i + \lambda_i}. \tag{1}$$

Analysis of experimental data in Fig. 2(b) yields $\lambda_i = 2.15$ mm, $\Lambda_i = 0.18$ mm, $c_i = 76$ μm/s, and $c_t = 6.1$ μm/s, which is in good agreement with the value of $c_t = 5.9$ μm/s predicted by Eq. (1).

Closer inspection of the transition region between merging and tracking reveals intriguing details that relate to the timing of propagation failures of the individual wave pulses. Figures 4(a)–4(d) show time-space plots obtained from experiments with pseudo-one-dimensional CHD-BZ systems. The initial concentration of bromate varies between $0.21M$ and $0.24M$ while all other concentrations and parameters are kept constant.

The time-space plots are complemented by graphs showing the time ΔT_n elapsed between the $(n-1)$st and the nth pulse death. At $[NaBrO_3]=0.21M$ (a), the pulses undergo propagation failures at an essentially constant period of 25 s and no leading wave pulse exists. Accordingly, we characterize these dynamics as simple tracking. However, at a slightly higher concentration of $[NaBrO_3]=0.22M$ (b), propagation failures occur according to a more complex rhythm, namely repeating sequences of two long ΔT_n values (26 s and 23 s) that are followed by a short value of about 8.5 s. At $[NaBrO_3]=0.23M$ (c), the rhythm follows a simpler short-long pattern (4.5 s and 30 s). Moreover, within the time-space plot every second pulse curls upward, thus indicating a prolonged lifetime of these pulses. At $[NaBrO_3]=0.24M$ (d), the system has reached simple merging that allows for the existence of a stable, slow moving frontier pulse. Furthermore, the rhythm of propagation failures has settled to a constant period of about 29 s.

More complex sequences of propagation failures can be observed for other bromate concentrations around the transi-

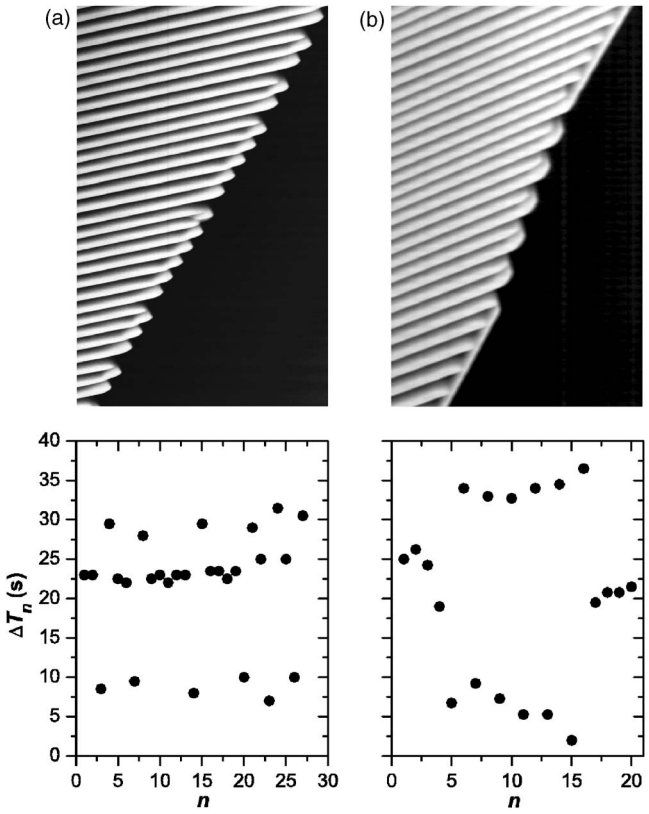

FIG. 5. Experimental space-time plots showing complex wave dynamics and corresponding analyses of ΔT_n. Initial concentrations as in Fig. 2(a) and 2(b) except $[NaBrO_3]=0.20M$ (a) and $0.22M$ (b). The horizontal and vertical axes span 5.4 mm and 600 s (a) and 8.6 mm and 450 s (b).

tion point. Unfortunately, they tend to be rather unstable and typically reveal no discernible pattern over the lifetime of the reaction system. We obtained, however, some satisfactory data from experiments with slightly different initial conditions. Two examples are shown in Fig. 5 in terms of time-space plots and their corresponding ΔT_n diagrams. The wave dynamics in (a) are dominated by a ΔT_n of about 23 s but also feature intermittent occurrences of pairs of short and long values (approximately 8 s and 30 s). The example in (b) is characterized by two distinct phases that are reminiscent of tracking with a simple short-long pattern and "pure" merging. The corresponding transitions are reminiscent of phase slips. In particular, it appears that the tracking-to-merging "switch" is triggered when the short period is nearly zero. This allows the next pulse to transform into a slow moving frontier pulse with long but finite lifetime. Moreover, one can clearly discern that the overall rate of pattern expansion during the merging type phase is larger than during the tracking type growth. This observation is in qualitative agreement with the data shown in Fig. 3.

IV. NUMERICAL RESULTS

In the following, we describe numerical simulations that aim to provide additional information on pulse dynamics in systems between merging and tracking. In particular, we demonstrate that complex sequences of propagation failures can be found in models of excitable reaction-diffusion systems.

Our simulations are based on a generic model of excitable reaction-diffusion media that involves one activator (u) and two inhibitor species (v, w),

$$\frac{\partial u}{\partial t} = \nabla^2 u + \frac{1}{\epsilon}\left(u(1-u)u - \frac{v+w}{a}\right), \tag{2}$$

$$\frac{\partial v}{\partial t} = u - v, \tag{3}$$

$$\frac{\partial w}{\partial t} = \beta(\delta - w) - \gamma u w, \tag{4}$$

where ϵ, a, β, δ, and γ are dimensionless constants. This model is an extension of the two-variable Barkley model [37] and has been used earlier to investigate various types of wave dynamics in excitable systems with anomalous dispersion [33]. Furthermore, it has similarities to more realistic models of the BZ reaction such as the Orgeonator [38,39] that describes the dynamics of the chemical key species bromous acid ($HBrO_2$), the oxidized form of the catalyst, and bromide ion (Br^-). However, our equations involve an additional source [$+\beta\delta$ in Eq. (4)] of bromide ion similar to certain modifications of the Oregonator model that aim to describe the inhibitory effects of molecular oxygen and/or light [40].

All simulations are performed for one-dimensional media with no-flux boundary conditions using Euler integration. Since systematic analyses require long computational runs, most of them are carried out on an IBM eServer pSeries 690 computer using OpenMP for parallelization. The time step and the grid spacing are typically 1×10^{-4} and 0.1, respectively or better. The typical system length and time interval simulated are 1000 and 500, respectively. Wave trains are created by perturbing the u value at the left boundary with a constant period to obtain continuously expanding systems. With the exception of δ, all model parameters are kept constant at $\epsilon=1.0\times10^{-2}$, $a=0.7$, $\beta=0.3$, and $\gamma=5.0$. However, we note that qualitatively similar phenomena are found for other sets of parameter values and, in particular, for the computationally more expensive case in which all three species undergo diffusion with equal or similar diffusion constants.

Figure 6 shows a sequence of time-space plots for six different values of the model parameter δ. Like in Fig. 4, these plots are complemented by diagrams showing the time elapsed between subsequent propagation failures. The initiation period is kept constant at $T_{ini}=5.0$. The data in Fig. 6(a) show a typical example of wave tracking where wave pulses vanish at a constant period. As the parameter δ is decreased, these simple dynamics give rise to more complex sequences of propagation failures and eventually lead to simple merging. Qualitatively, these numerical results are in very good agreement with our experimental findings. Two of the numerical simulations, which could be observed experimentally in a stable pattern, are the dynamics with two tracking events followed by one merging event [see Fig. 4(b) and Fig. 6(c)]

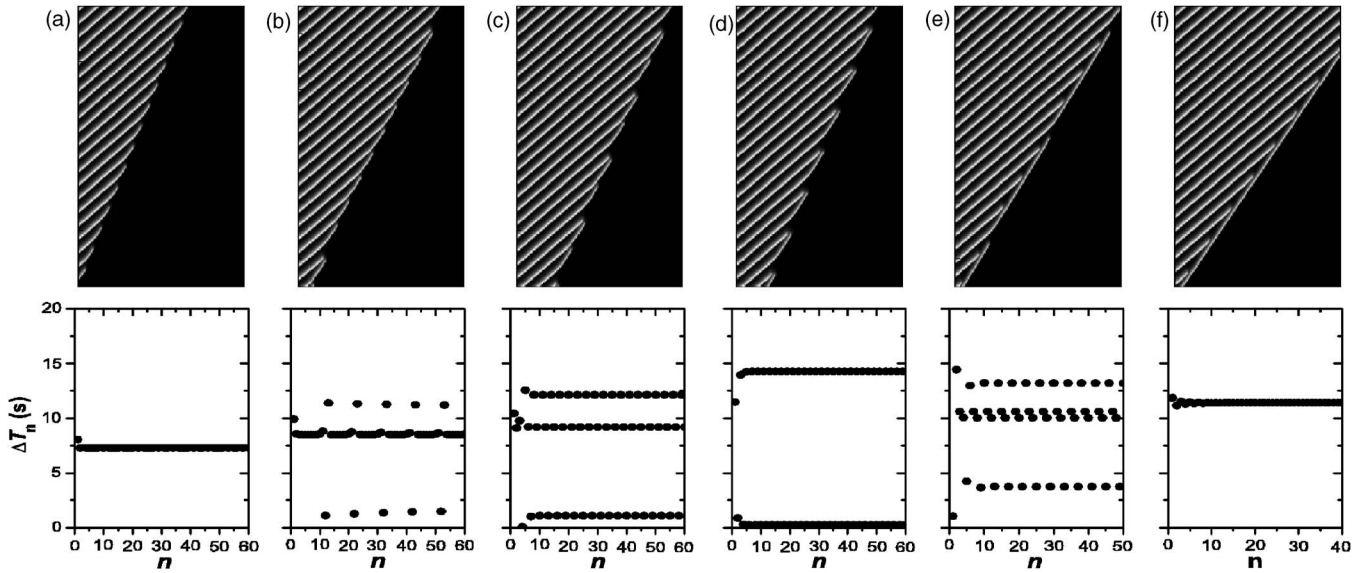

FIG. 6. Numerically obtained space-time plots and their corresponding ΔT_n diagrams for the following δ-values: 0.2700 (a), 0.2670 (b), 0.2666 (c), 0.2660 (d), 0.2652 (e), and 0.2640 (f). The horizontal space and vertical time axes span 150 and 100 units, respectively. Wave trains are created at a constant period of 5.0. The other numerical parameters are $a=0.7$, $\beta=0.3$, $\epsilon=10^{-2}$, and $\gamma=5.0$.

as well as the alternating short-long pattern [see Fig. 4(c) and Fig. 6(d)].

Figure 7 shows a plot of the ΔT_n dependence on the parameter δ. Within the narrow transition interval, we find simple period-1 merging and simple period-1 tracking for the smallest and the largest δ values, respectively. The most pronounced transition state exists around $\delta=0.2660$, which is characterized by a simple short-long rhythm similar to dynamics shown in Fig. 6(d). This rhythm persists from $\delta=0.2653$ to $\delta=0.2664$. About halfway through this interval, the ΔT_n values show a striking cusp that occurs when the short-period branch approaches zero. We note that this feature is caused by a simple reversal in the order of propagation failures: on the right-hand side of the cusp (i.e., the high δ, tracking type side) the pulses undergo propagation failures according to their order of initiation. On the left-hand side (i.e., the low δ, merging type side), however, pulses vanish according to the sequence "2,1,4,3,6,5,…," where the numbers denote the order of pulse initiation.

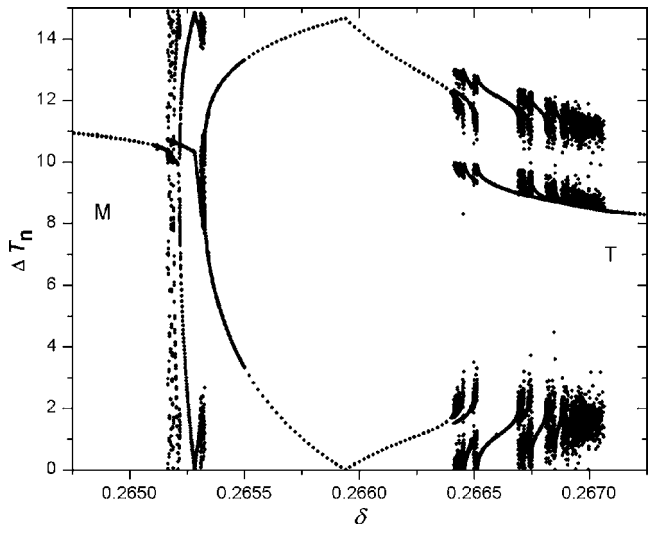

FIG. 7. Numerical results of the ΔT_n dependence on the parameter δ revealing a variety of dynamical states in the transition between the merging (M) and the tracking (T) regime. All numerical parameters are the same as in Fig. 6.

In addition to the simple short-long rhythm, we find period-3 and period-4 patterns around $\delta=0.2666$ and $\delta=0.2668$, respectively. Other intricate patterns as well as possible examples of aperiodic and chaotic behavior are also discernible, but they are found in much narrower intervals of our bifurcation parameter δ. This finding is in good, qualitative agreement with our experimental measurements that yielded robust period-1, period-2, and period-3 patterns (cf. Fig. 4) while all other patterns were highly susceptible to small changes of the system (cf. Fig. 5).

To obtain further insights into the dependencies controlling the dynamics of propagation failures, we study the pulse evolution as a function of the wave train's initiation period T_{ini}. Notice that all simulations above were carried for $T_{\mathrm{ini}}=5.0$. Figure 8 shows the bifurcation diagram of ΔT_n with respect to the period of pulse initiation. All system parameters are identical to the values specified above and $\delta=0.2660$ which, at $T_{\mathrm{ini}}=5.0$, corresponds to the simple short-long pattern shown in Fig. 6(d). Moreover, the data in Fig. 8 are compiled from the propagation failures of 20 consecutive waves starting with the sixth wave. The first five periods are ignored to avoid transients and possible artifacts caused by the specific perturbation employed in the initiation of the pulses. Such atypical behavior is clearly discernible in Fig. 6 and was also excluded before generating the bifurcation diagram in Fig. 7.

As expected, the results in Fig. 8 reveal simple short-long rhythms for initiation periods around 5.0. Pulse initiations at periods below $T_{\mathrm{ini}}\approx 3.5$ fail to generate a pulse for every perturbation because the given system is unable to support

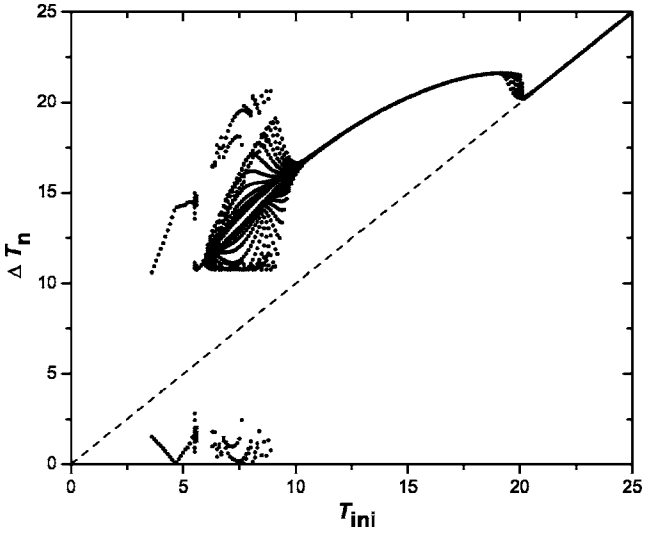

FIG. 8. ΔT_n dependence on the parameter T_{ini} at $\delta=0.2660$. All other numerical parameters are the same as in Fig. 6. The dashed line indicates $\Delta T_n = T_{\mathrm{ini}}$.

such high-frequency wave trains. Between $T_{\mathrm{ini}} \approx 5.4$ and $T_{\mathrm{ini}} \approx 10$, complex patterns are observed that involve numerous ΔT_n values. The latter values are mainly above $\Delta T_n = 10$ and only few are below 3, which creates the impression of a forbidden window at intermediate values of ΔT_n. For even longer initiation periods ($T_{\mathrm{ini}} \approx 10-20$), we find predominantly period-1 behavior with ΔT_n values that are significantly larger than T_{ini}. The difference between the rate of propagation failure and the rate of pulse initiation is simply caused by the expansion of the wave train. For even larger values of T_{ini}, this difference vanishes and wave initiation fails to create an expanding wave pattern.

V. CONCLUSIONS

In conclusion, we have presented the first evidence for complex rhythms caused by propagation failures of finite wave trains in reaction-diffusion media. These complex rhythms are found within the transition region between different forms of expanding pulse trains. Specifically, this paper focused on the transition between wave merging and tracking, but preliminary experimental and numerical results indicate that similar phenomena also exist for the transition between wave stacking and merging. One experimental example of the latter transition behavior is shown in Fig. 9. After five stacking events, two fronts merge with their preceding wave at $t=55$ s and $t=135$ s (indicated by the horizontal arrows), followed by other stacking events.

All of these different wave dynamics were discovered only recently and they result from anomalies in the system's dispersion relation [21–23,33,34,41]. In this context it is important to emphasize that these so-called anomalies are the normal case for important, although understudied, classes of excitable media such as systems with a stable, focuslike steady state. Moreover, very similar phenomena exist during the propagation of charge densities in semiconductor superlattices [42].

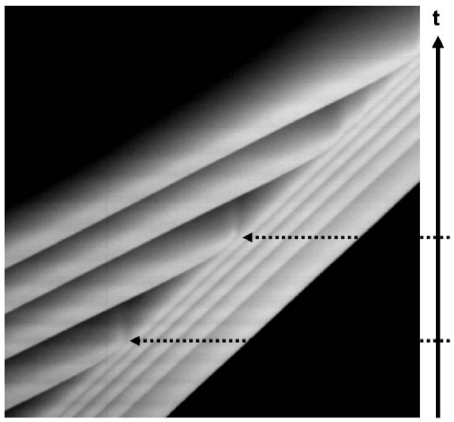

FIG. 9. Space-time plot of wave dynamics in the transition region between merging and stacking. Initial concentrations: $[H_2SO_4]=0.6M$, $[CHD]=0.11M$, $[NaBrO_3]=0.15M$, and [ferroin] $=0.5$ mM. The horizontal and vertical axes span 13 mm and 300 s.

The various rhythms of propagation failures reported in this study show a remarkable variety. Although the most abundant patterns are the period-1, period-2, and period-3 rhythms, we also found more complex examples as well as indications for aperiodic and chaotic behavior. The overall dynamics share many similarities with purely temporal systems such as coupled oscillators and media with mixed-mode oscillations [43]. These temporal systems have been extensively studied in chemical, electrochemical and biological systems and their analyses usually employ concepts such as firing numbers and Farey sequences. Despite many similarities it appears that there is a wealth of new phenomena to be discovered in the context of propagation failures; especially if one includes wave trains in two- and three-dimensional systems. Moreover, the propagation failures in our system are truly spatio-temporal in nature and affect spatial aspects such as the overall expansion of the wave train.

Last, we emphasize that our results are not limited to chemical reaction-diffusion media, but similar dynamics are expected to exist in a much broader spectrum of experiments. In particular, it will be interesting to explore these complex, transition dynamics in other, physical and biological, systems with nonmonotonic dispersion relations. These systems include but are not limited to excitable neuronal and cardiac tissue in which excitation waves are carriers of biologically relevant information.

ACKNOWLEDGMENTS

This work was supported by the Chemistry Division of the National Science Foundation (Grant No. CHE-0513912). The authors thank the FSU School for Computational Science and Information Technology (CSIT) for allowing the use of their IBM pSeries 690 Power4-based supercomputer "Eclipse." One of the authors (N.M.) thanks the "Deutsche Akademie für Naturforscher Leopoldina" (Grant No. BMBF-LPD 9901/8-85) for financial support.

[1] S. K. Scott, *Chemical Chaos* (Clarendon, Oxford, 1991).
[2] *Growth and Perfection of Crystals*, edited by R. H. Deremus, B. W. Roberts, and D. Turnbull (Wiley, New York, 1958).
[3] D. Kandel and J. D. Weeks, Phys. Rev. Lett. **69**, 3758 (1992).
[4] V. I. Koroleva and J. Bureš, Brain Res. **173**, 209 (1979).
[5] B. T. Grenfell, O. N. Bjørnstad, and J. Kappey, Nature (London) **414**, 716 (2001).
[6] N. Suzuki, M. Hirata, and S. Kondo, Proc. Natl. Acad. Sci. U.S.A. **100**, 9680 (2003).
[7] *Chemical Waves and Patterns*, edited by R. Kapral and K. Showalter (Kluwer, Dordrecht, Netherlands, 1995).
[8] A. T. Winfree, Science **175**, 634 (1972).
[9] D. Barkley, Phys. Rev. Lett. **72**, 164 (1994).
[10] K. I. Agladze, V. I. Krinsky, A. V. Panfilov, H. Linde, and L. Kuhnert, Physica D **39**, 38 (1989).
[11] J. J. Tyson and J. P. Keener, Physica D **53**, 151 (1991).
[12] J. M. Davidenko, A. V. Pertsov, R. Salomonsz, W. Baxter, and J. Jalife, Nature (London) **355**, 349 (1992).
[13] R. A. Gray, A. M. Pertsov, and J. Jalife, Nature (London) **392**, 75 (1998).
[14] D. F. Tatterson and J. L. Hudson, Chem. Eng. Commun. **1**, 3 (1973).
[15] O. Steinbock and S. C. Müller, Physica A **188**, 61 (1992).
[16] J.-M. Flesselles, A. Belmonte, and V. Gáspár, J. Chem. Soc., Faraday Trans. **94**, 851 (1998).
[17] C. Elphick, E. Meron, and E. A. Spiegel, Phys. Rev. Lett. **61**, 496 (1988).
[18] C. Elphick, E. Meron, J. Rinzel, and E. A. Spiegel, J. Theor. Biol. **146**, 249 (1990).
[19] S. Jakubith, H. H. Rotermund, W. Engel, A. von Oertzen, and G. Ertl, Phys. Rev. Lett. **65**, 3013 (1990).
[20] J. Christoph, M. Eiswirth, N. Hartmann, R. Imbihl, I. Kevrekidis, and M. Bär, Phys. Rev. Lett. **82**, 1586 (1999).
[21] N. Manz, S. C. Müller, and O. Steinbock, J. Phys. Chem. A **104**, 5895 (2000).
[22] C. T. Hamik, N. Manz, and O. Steinbock, J. Phys. Chem. A **105**, 6144 (2001).
[23] C. T. Hamik and O. Steinbock, Phys. Rev. E **65**, 046224 (2002).
[24] H. Zhang and A. V. Holden, Math. Biosci. **188**, 175 (2004).
[25] K. S. Ramaiah, I. Bhat, T. P. Chow, J. K. Kim, and E. F. Schubert, J. Appl. Phys. **98**, 106108 (2005).
[26] B. J. Gibbons, J. Noffsinger, and J. P. Pelz, Surf. Sci. **575**, L51 (2005).
[27] M. J. Krasiński and R. Rolandi, J. Cryst. Growth **169**, 548 (1996).
[28] V. I. Bredikhin, G. L. Galushkina, A. A. Kulagin, S. P. Kuznetsov, and O. A. Malshakova, J. Cryst. Growth **259**, 309 (2003).
[29] K. Pond, A. C. Gossard, A. Lorke, and P. M. Petroff, Mater. Sci. Eng., B **30**, 121 (1995).
[30] S. Lee, M. Akabori, T. Shirahata, K. Takada, J. Motohisa, and T. Fukui, J. Cryst. Growth **231**, 75 (2001).
[31] G. Bordiougov and H. Engel, Phys. Rev. Lett. **90**, 148302 (2003).
[32] M. Falcke, M. Or-Guil, and M. Bär, Phys. Rev. Lett. **84**, 4753 (2000).
[33] N. Manz, C. T. Hamik, and O. Steinbock, Phys. Rev. Lett. **92**, 248301 (2004).
[34] N. Manz and O. Steinbock, J. Phys. Chem. **108**, 5295 (2004).
[35] K. Kurin-Csörgei, A. M. Zhabotinsky, M. Orbán, and I. R. Epstein, J. Phys. Chem. **100**, 5393 (1996).
[36] K. Kurin-Csörgei, A. M. Zhabotinsky, M. Orbán, and I. R. Epstein, J. Phys. Chem. A **101**, 6827 (1997).
[37] D. Barkley, Physica D **49**, 61 (1991).
[38] R. J. Field and R. M. Noyes, J. Chem. Phys. **60**, 1877 (1974).
[39] J. J. Tyson and P. C. Fife, J. Phys. Chem. **73**, 2224 (1980).
[40] H.-J. Krug, L. Pohlmann, and L. Kuhnert, J. Phys. Chem. **94**, 4862 (1990).
[41] N. Manz and O. Steinbock, Phys. Rev. E **70**, 066213 (2004).
[42] A. Amann and E. Schöll, J. Stat. Phys. **119**, 1069 (2005).
[43] S. K. Scott and A. S. Tomlin, Philos. Trans. R. Soc. London, Ser. A **332**, 51 (1990).